Computer Vision and Image Understanding 151 (2016) 3–13

Contents lists available at ScienceDirect

Computer Vision and Image Understanding

journal homepage: www.elsevier.com/locate/cviu

Modeling 4D pathological changes by leveraging normative models

Bo Wang[a,b,*], Marcel Prastawa[c], Andrei Irimia[d], Avishek Saha[e], Wei Liu[a,b], S.Y. Matthew Goh[d], Paul M. Vespa[f], John D. Van Horn[d], Guido Gerig[g]

[a] Scientific Computing and Imaging Institute, University of Utah, 72 Central Campus Drive, Salt Lake City, UT 84112 USA
[b] School of Computing, University of Utah, 50 S., Central Campus Drive, Salt Lake City, UT 84112 USA
[c] Icahn School of Medicine at Mount Sinai, 1468 Madison Avenue, New York, NY 10029 USA
[d] The Institute for Neuroimaging and Informatics, Keck School of Medicine, University of Southern California, 2001 North Soto Street, Los Angeles CA 90089 USA
[e] Yahoo Labs, 701 1st Ave, Sunnyvale, CA 94089 USA
[f] Brain Injury Research Center, Department of Neurosurgery, David Geffen School of Medicine, University of California, Los Angeles, CA 90095 USA
[g] Tandon School of Engineering, Department of Computer Science and Engineering, NYU, USA

ARTICLE INFO

Article history:
Received 16 February 2015
Accepted 18 January 2016

Keywords:
Image segmentation
Brain parcellation
Medical imaging

ABSTRACT

With the increasing use of efficient multimodal 3D imaging, clinicians are able to access longitudinal imaging to stage pathological diseases, to monitor the efficacy of therapeutic interventions, or to assess and quantify rehabilitation efforts. Analysis of such four-dimensional (4D) image data presenting pathologies, including disappearing and newly appearing lesions, represents a significant challenge due to the presence of complex spatio-temporal changes. Image analysis methods for such 4D image data have to include not only a concept for joint segmentation of 3D datasets to account for inherent correlations of subject-specific repeated scans but also a mechanism to account for large deformations and the destruction and formation of lesions (e.g., edema, bleeding) due to underlying physiological processes associated with damage, intervention, and recovery.

In this paper, we propose a novel framework that provides a joint segmentation-registration framework to tackle the inherent problem of image registration in the presence of objects not present in all images of the time series. Our methodology models 4D changes in pathological anatomy across time and also provides an explicit mapping of a healthy normative template to a subject's image data with pathologies. Since atlas-moderated segmentation methods cannot explain appearance and locality pathological structures that are not represented in the template atlas, the new framework provides different options for initialization via a supervised learning approach, iterative semisupervised active learning, and also transfer learning, which results in a fully automatic 4D segmentation method.

We demonstrate the effectiveness of our novel approach with synthetic experiments and a 4D multimodal MRI dataset of severe traumatic brain injury (TBI), including validation via comparison to expert segmentations. However, the proposed methodology is generic in regard to different clinical applications requiring quantitative analysis of 4D imaging representing spatio-temporal changes of pathologies.

1. Introduction

Quantitative studies in longitudinal image data from traumatic brain injury (TBI), autism, and Huntington's disease, for example, are important for assessment of treatment efficacy, monitoring disease progression, or making predictions on outcome. In this paper, we will use the term '*pathological anatomy* to indicate image data that represent pathologies and lesions and therefore differ from normative anatomical templates that encode healthy anatomy. The modeling of four-dimensional (4D) pathological anatomy is essential to understand the complex dynamics of pathologies and enables other analyses such as structural pathology [1] and brain connectivity [2]. Modeling pathological changes is a challenging task because of the difficulties in localizing multiple lesions at specific time points and estimating deformations across time points with changing lesion patterns. Such modeling involves solving interdependent segmentation and image registration since registration needs to know about areas of pathology but 4D segmentation requires an intrasubject mapping across time points.

* Corresponding author was at: School of Computing, University of Utah, 50 S., Central Campus Drive, Salt Lake City, UT 84112 USA. Bo Wang is with the GE Global Research Center, Niskayuna, NY 12309 USA
E-mail address: bowang@cs.utah.edu (B. Wang).

http://dx.doi.org/10.1016/j.cviu.2016.01.007
1077-3142/

Furthermore, subject-specific registration across time points is not sufficient to segment pathological anatomy if we follow the well-established concept of atlas-driven segmentation, which includes probabilistic tissue priors for a Bayesian maximum posterior classification. Such a scheme requires an explicit registration from a normative template atlas to each subject's image time point, with the additional advantage of using anatomical labeling of subregions as used in brain connectivity analysis, for example.

The main goal of this paper therefore is the development of a new 4D pathological anatomy modeling framework that simultaneously solves segmentation of each time point and also estimates nonlinear deformations to a normative atlas space and across time points. We will use severe TBI as our clinical driving problem to demonstrate the different components of the novel method and to validate results in comparison to human expert segmentations. TBI is not only a critical problem in healthcare that impacts approximately 1.7 million people in the United States every year [3], but also one of the most challenging tasks for quantitative image-based interpretation and analysis. The varying causes (falls, car accidents, etc.) and degrees of TBI present highly heterogeneous multifocal patterns of lesions with largely variable morphometry. Spatio-temporal analysis of serial TBI imaging is motivated by the clinical need for improved insight and quantitative data from therapeutic intervention and rehabilitation that change brain neuroanatomy and function with a reduction/cessation of symptoms.

2. Related work/previous work

4D pathological anatomy modeling is closely related to longitudinal image analysis, a research area of increasing interest to the scientific community due to the availability and use of longitudinal imaging in medical research and clinical practice.

Researchers have proposed different methods for longitudinal image/shape analysis [4–8]. These image regression methods were developed for image data resembling normal anatomy with small-scale temporal deformations. However, these methods are not designed for pathological anatomy presenting nondiffeomorphic deformations and topological changes due to spatio-temporal lesion evolution. In the following sections, we discuss previous work related to pathological brain MR image analysis, organized by the type of problem to be solved.

2.1. 3D/4D segmentation

One class of work focuses on 3D volume data segmentation [9–13]. Menze et al. [9] presented a generative model for brain tumor segmentation using multimodal MR images. Geremia et al. [10] proposed to use random forests for automatic segmentation of multiple sclerosis (MS) lesions in multimodal MR images. Bauer et al. [11] presented an automatic segmentation method based on support vector machine classification with smoothness constraints. Gao et al. [12] developed a robust statistics-based interactive multiobject segmentation tool. Ledig et al. [13] proposed a method based on the Gaussian mixture modeling (GMM) with patch-based spatially and temporally varying constraints to enforce temporal coupling. All these methods use different classifiers with different image-derived features as input or even incorporate temporal information for pixel classification, but they are not designed for longitudinal pathological anatomy studies due to the lack of intra- and intersubject registration.

Atlas-based segmentation has been demonstrated to be a powerful solution in the case of segmenting healthy or normal-looking brain MR images [14]. In scenarios where pathological structures are present in the subject image but not in the atlas, this method could be extended to a GMM-based approach where an affine-registered atlas and user initialization are combined [15].

2.2. Intrasubject registration

A second class of methods is concerned with registration across time points [16–19]. Chitphakdithai and Duncan [16] proposed a registration method accommodating the missing correspondences for preoperative and post-resection brain images. Niethammer et al. [17] presented a registration framework for TBI images using geometric metamorphosis that maps TBI over time using known, presegmented lesion boundaries defined manually. Ou et al. [18] proposed a generic deformable registration method using attribute matching and mutual-saliency weighting. Lou et al. [19] presented a deformable registration method for intra-time point multimodal image registration. However, these image-registration methods describe deformations but do not provide segmentation of anatomical structures.

2.3. Pathological anatomy growth model

A third class of methods focuses on modeling the growth of pathological anatomy such as tumor or glioma [20–24]. Kyriacou et al. [20] proposed a finite element-based biomechanical model for registering a normal atlas to a patient image. Cuadra et al. [21] developed an atlas-based segmentation method using a lesion growth model. Zacharaki et al. [22] proposed a multiresolution method that utilized a principal component analysis (PCA)-based model of tumor growth for deformable registration of brain tumor images. Gooya et al. [24] presented a segmentation and registration method for MR images of glioma patients using a tumor growth model. Menze et al. [23] proposed a generative model of tumor growth and image appearance that relies on modeling the pathophysiological process and data likelihood. These methods provide a segmentation of pathological anatomy or mapping from an atlas to the pathological data but do not include intrasubject registration for a full 4D modeling of healthy and pathological structures.

2.4. Joint segmentation and registration

A fourth class of methods is joint segmentation and registration [25–28]. Pohl et al. [25] proposed a Bayesian framework for joint segmentation and registration for normal brain MR images. Parisot et al. [26] proposed a tumor segmentation and registration method to solve brain tumor segmentation and atlas to patient image registration simultaneously by using a Markov random field model with a sparse grid. Kwon et al. [27] developed a deformable tumor registration tool for preoperative and postrecurrence brain MR scans. Liu et al. [28] proposed a low-rank image decomposition-based atlas registration method to map a healthy brain atlas to a patient image. These methods approach problems similar to those discussed in this paper but focus on one subproblem such as atlas registration [28], intrasubject registration [27], and tumor segmentation with atlas registration [26] rather than a combined, joint framework.

2.5. Novel methodological framework

Although significant progress has been demonstrated in various aspects of methods for longitudinal pathological image analysis, we propose a solution that includes the remaining open issues related to multimodal image analysis and longitudinal modeling. The processing framework includes explicit mapping from a normative probabilistic template representing healthy anatomy to each image of the subject's image time series and multimodal segmentation and extends early work [29] in which we focused on a pathological anatomy modeling framework with transfer learning-based image appearance model estimation by adding user initialization and user

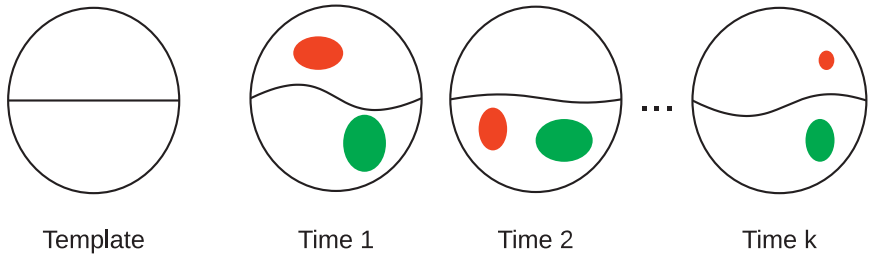

Fig. 1. Motivation and challenges in 4D pathological anatomy modeling. Given a time series of image data, we show deformable lesions that can be modeled by diffeomorphic registration (green) but also disappearing and newly appearing lesions across time. The normative template (left) does not provide prior information on lesion type and locality. (For interpretation of the references to color in this figure legend, the reader is referred to the web version of this article.)

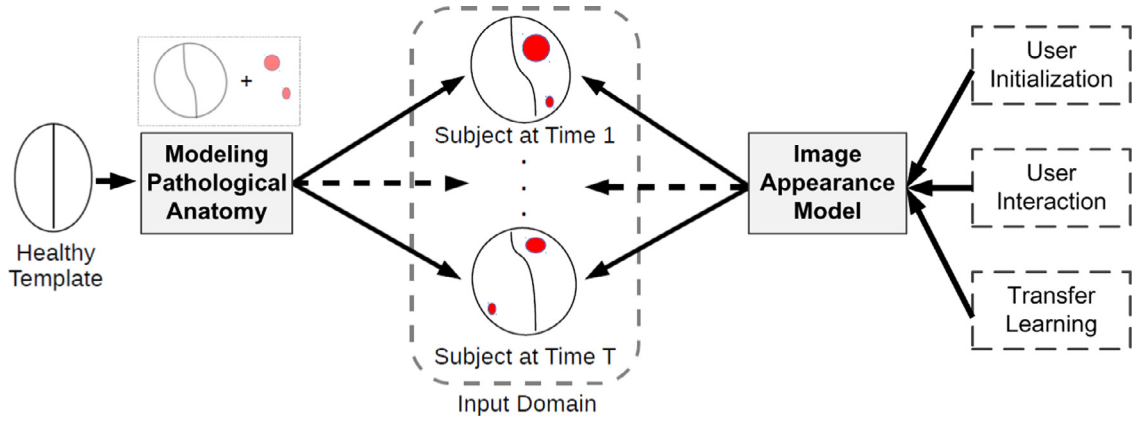

Fig. 2. Conceptual overview of the proposed framework. To provide a spatial context for the 4D modeling, the method maps a healthy template to input images of a subject at different time points. For initialization of the image appearance model, we provide different machine learning approaches from semisupervised methods such as user initialization or iterative user interaction to fully automatic transfer learning.

interaction as alternative approaches to estimate the image appearance model. We also present a study of manual expert annotation comparison by having three human experts perform manual segmentation using the latest version of ITK-SNAP 3.2.0 [30], which is to our knowledge the only tool available to take multimodal data as input for performing manual segmentation.

3. Method

3.1. Motivation and challenges

Image registration schemes often assume preservation of topology and point-to-point correspondences and therefore apply diffeomorphic registration schemes, assumptions that are clearly violated in the presence of newly appearing and disappearing lesion patterns. Fig. 1 shows a toy example with two classes of changes between different time points. The first class of changes is described by the expanding or shrinking of existing structures, which is simply geometric change. The second class of changes is given by disappearing or newly appearing structures, resulting in changes of topology.

3.2. 4D modeling of pathological anatomy

The previous example illustrates the core motivation for the proposed methodology, which is a concept to provide nonlinear registration and 4D segmentation in the presence of changes in topology.

We propose a processing scheme that constructs 4D models of pathological anatomy including a prior from a normative template and describes changes at different time points to provide a complete 4D segmentation of normal tissue and pathologies. Fig. 2 shows a conceptual overview of our framework.

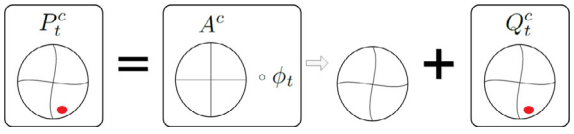

Fig. 3. Illustration of the basic concept. Class-specific posteriors at a specific time point t are modeled as a combination of a diffeomorphic deformation of a normative template and a nondiffeomorphic probability.

We model anatomical changes over time as a combination of diffeomorphic image deformation and nondiffeomorphic changes of probabilities for lesion categories, accounting for temporally smooth deformations and abrupt changes due to lesions appearing and disappearing over time, for example. Specifically, the spatial prior P_t^c for each class c at time point t is modeled as

$$P_t^c = A^c \circ \phi_t + Q_t^c \tag{1}$$

where A is the tissue class probability that is initially associated with the healthy template, ϕ_t is the diffeomorphic deformation from time t to the atlas, and Q_t is the nondiffeomorphic probabilistic change for time t. The method estimates a common subject-specific atlas A for all time points. Fig. 3 shows a conceptual view of the two components.

Given the model and 4D multimodal images I_t at time points t, we estimate model parameters that minimize the following functional:

$$\begin{aligned} &\underset{A,\phi_t,Q_t,\theta_t}{\operatorname{argmin}}\ \mathcal{F}(A,\phi_t,Q_t,\theta_t) + \mathcal{R}_1(Q) + \mathcal{R}_2(A) + \mathcal{R}_3(\phi) \\ &\text{s. t.} A^c \in [0,1],\ \sum_c A^c = 1,\ (A^c \circ \phi_t + Q_t^c) \in [0,1], \\ &\sum_c (A^c \circ \phi_t + Q_t^c) = 1 \end{aligned} \tag{2}$$

where $\mathcal{F}$ represents the data functional (the negative total log-likelihood)

$$\mathcal{F}(A, \phi_t, Q_t) = -\sum_{t=1}^{T}\sum_{x=1}^{N} \log\left(\sum_{c=1}^{C} P_t^c(x)\, p(I_t(x)|c, \theta_t^c)\right), \tag{3}$$

and $\mathcal{R}$ represents the regularity terms:

$$\mathcal{R}_1(Q) = \alpha \sum_t \| Q_t \|_{L_1}, \quad \mathcal{R}_2(A) = \beta \| A - A^{(0)} \|_{L_2},$$
$$\mathcal{R}_3(\phi) = \gamma \sum_t d(id, \phi_t). \tag{4}$$

T denotes the number of observed time points, C denotes the number of tissue classes, $p(I_t|c, \theta_t^c)$ is the image likelihood function for class c with parameter θ_t^c, $A^{(0)}$ is the initial atlas A obtained from the healthy template, and $d(id, \cdot)$ is the distance to the identity transform. $\mathcal{R}_1$ enforces the sparsity of Q, $\mathcal{R}_2$ prevents extreme deviations in A from the initial model, and $\mathcal{R}_3$ enforces the smoothness of the deformations ϕ_t. These regularization functionals are weighted by user-defined parameters α, β, γ, respectively.

The model parameters $\{A, \phi_t, Q_t\}$ are obtained via gradient descent and the initial image likelihoods of the multimodal input image data, $p(I_t|c, \theta_t^c)$ are obtained via an initialization scheme as discussed later. We use multimodal image intensities as our feature vector, $I_t(x) = [I_1(x), I_2(x), \ldots, I_k(x)]_t$.

3.3. Image appearance model

Given multimodal images $I_t = \{I(x_1), \ldots, I(x_N)\}_t$ at time point t with N voxels indexed by positions x and M_t number of channels, we estimate the parameters of $p(I_t|c, \theta_t^c)$ that maximize the log-likelihood function for each time point t as

$$\sum_x \log \sum_{c=1}^{C_t} p(I_t(x)|\theta_t^c)\Pi_t^c(x), \tag{5}$$

where C_t is the number of classes at time point t, and Π_t^c is the spatial prior for class c at time t.

In order to estimate the image appearance model, we provide flexible choices for initialization via different machine learning approaches (see Section 3.5). Depending on the machine learning approaches we use for image appearance modeling, $p(I_t(x)|\theta_t^c)$ is either $p(I_t(x)|\mu_t^c, \Sigma_t^c)$, the multivariate Gaussian probability distribution with mean μ_t^c and covariance Σ_t^c, for user initialization (Section 3.5.1) and iterative user interaction (Section 3.5.2), or the kernel density model parameterized by the kernel bandwidths for each class $\theta_t = \{h^{c=1}, \ldots, h^{c=C}\}$ for transfer learning (Section 3.5.3).

3.4. Model parameter estimation

We perform model parameter estimation by minimizing the overall objective function (Eq. (2)) with respect to each parameter using alternating gradient descent. In particular, we use these gradient equations to optimize the data functional $\mathcal{F}$:

$$\nabla_{Q_t^c}\mathcal{F}(x) = -\frac{p(I_t(x)|c, \theta_t^c)}{\sum_{c'} P_t^{c'}(x)\, p(I_t(x)|c', \theta_t^{c'})}, \tag{6}$$

$$\nabla_{A^c}\mathcal{F}(x) = -\sum_t \frac{|D\,\phi_t(x)|\, p(I_t(\phi_t^{-1}(x))|c, \theta_t^c)}{\sum_{c'}(A^{c'}(x) + Q_t^{c'}(\phi_t^{-1}(x)))\, p(I_t(\phi_t^{-1}(x))|c', \theta_t^{c'})}, \tag{7}$$

$$\nabla_{\phi_t}\mathcal{F}(x) = -\sum_c \frac{p(I_t(x)|c, \theta_t^c)}{\sum_{c'} P_t^{c'}(x)\, p(I_t(x)|c', \theta_t^{c'})} \nabla(A^c \circ \phi_t(x)), \tag{8}$$

where $|D\phi|$ denotes the determinant of the Jacobian of ϕ. The updates show that Q_t moves to the data likelihood specific to time t, A moves to the average data likelihood over time, and ϕ_t deforms A to match the boundaries between data and atlas. Please refer to Appendix A for the derivations of Eqs. (6)–(8). Constraints are enforced using projected gradient descent [31]). The image likelihood model $p(I_t|c, \theta_t^c)$ obtained from the image appearance model is fitted to the input image data using gradient descent update $\nabla_{\theta_t^c}\mathcal{F}$, which finds the parameter θ_t^c that best matches data to the current atlas $P_t^c = A^c \circ \phi_t + Q_t^c$. The algorithm for model parameter estimation is shown in Algorithm 1.

Algorithm 1 Algorithm for constructing 4D anatomical model.

Input: multimodal images $I_t(x)$, **healthy brain atlas** A.
Output: segmentations Z_t^c and deformations ϕ_t.
Repeat until convergence
1: $Q_t^c \leftarrow Q_t^c - \epsilon\nabla_{Q_t^c}\mathcal{F} + \mathcal{R}_1$
2: $A^c \leftarrow A^c - \epsilon\nabla_{A^c}\mathcal{F} + \mathcal{R}_2$
3: $\phi_t \leftarrow \phi_t - \epsilon\nabla_{\phi_t}\mathcal{F} + \mathcal{R}_3$
5: θ_t^c: $\leftarrow \theta_t^c - \epsilon\ \nabla_{\theta_t^c}\mathcal{F}$
Final segmentation $Z_t^c \leftarrow \frac{A_t^c\, p(I_t|c)}{\sum_{c'} A_t^{c'}\, p(I_t|c')}$

3.5. Machine learning-based image appearance model estimation

Standard atlas-based methods are not suitable to estimate the image appearance model for pathological data since the lesion locations and appearance are not represented in the atlas. For example, standard normative brain atlases contain priors of white matter (WM), gray matter (GM), and cerebrospinal fluid (CSF) but cannot explain lesions such as edema, necrosis, and bleeding. The method proposed here includes the segmentation and modeling of pathology but requires an initialization of the multimodal appearance parameters. We propose several options for such initialization that may be suitable for different scenarios and application domains. Semisupervised machine learning methods offer semiautomatic solutions by asking the user to provide training data through initialization or interaction. Transfer learning offers a fully automatic solution by leveraging labeled data in one domain to learn a classifier for data in another domain where training data is not available. We discuss a supervised learning method in Section 3.5.1, a semisupervised learning method in Section 3.5.2, and a transfer learning method in Section 3.5.3.

3.5.1. User initialization

A common procedure for supervised classification is to let a user define regions of interest of the different types of pathology categories in an affine-registered normative atlas, for example by drawing spherical regions for lesion types [32,33]. The expert input, number of lesion types, and an affine-registered atlas are then used to initialize the parameters of the multivariate Gaussian probability distribution (μ_t^c and $\mathbf{\Sigma}_t^c$), and spatial prior Π_t^c via these user-input spheres S_t for each tissue/lesion class $c = 1, \ldots, k_t, k_l, \ldots, K$ where $c = 1, \ldots, k_t$ are normal tissue classes and $c = k_l, \ldots, K$ are lesion classes. We use the K-means algorithm [34] to get initial estimates μ_t^c and $\mathbf{\Sigma}_t^c$ for each lesion class $c = k_l, \ldots, K$. For normal tissue classes $c = 1, \ldots, k_t$, we use the affine-registered atlas (masked by user input S_t) to estimate μ_t^c and $\mathbf{\Sigma}_t^c$. The initial priors Π_t^c for each class are obtained by modifying the standard atlas using S_t. We assume that lesions are found in a subset of normal tissue classes $L \subseteq c = 1, \ldots, k_t$, which depends on the specific applications, so that the initial prior for each lesion class becomes $\Pi_t^c = w(\sum_{n\in L}\Pi_t^n) + S_t$, for $c = k_l, \ldots, K$, where w is a uniform weight for lesions chosen to be a small value (0.001 for example). The Π_t^c of other classes are linearly transformed to ensure that $\sum_{c=1}^{K}\Pi_t^c = 1$ at each location.

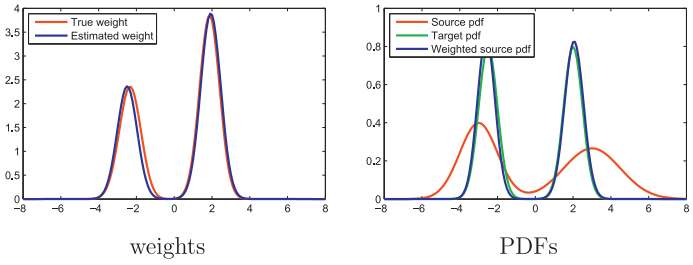

Fig. 4. Toy example to illustrate estimation of weights using KLIEP.

3.5.2. Iterative user interaction: ActiveCut

A second way to estimate the image appearance model is to use iterative user interaction following an ActiveCut scheme [35]. Given a user-defined bounding box, the hard-constraint map is set to 'normal' outside the box and 'uncertain' inside. Then, we initialize an α map such that $\alpha=1$ (lesion) in the 'uncertain' region of the hard-constraint, and $\alpha=0$ elsewhere. The expectation-maximization (EM) algorithm learns θ of both foreground and background GMMs given α, and then a graph-cut step [36] updates only the α for voxels within the 'uncertain' region. This update strategy of graph-cuts prevents false-positive detections. Upon EM and graph-cuts convergence, there may be some false-negative voxels in 'normal' regions. We group these voxels into spatially coherent objects and find the one with the highest score computed from certain criteria. The algorithm either automatically adds the candidate to lesions or queries the user for an answer, depending on its confidence in the candidate. We then update the hard-constraint map to reflect the knowledge learned from the new object, and a new EM and graph-cuts iteration starts. Objects already accepted or rejected in previous steps are recorded so they will be excluded from future queries. This learning process repeats until the user stops the algorithm, and the image appearance parameters are then used to initialize to the 4D segmentation scheme as discussed previously.

3.5.3. Transfer learning

A third approach is the use of transfer learning following [29], a procedure that does not require any user input and thus results in a fully automatic processing scheme. We compute the image appearance model $p(I_t|c,\theta_t^c)$ using domain adaptation, where we adapt an appearance model from a known domain (here tumor image database with labelled data) to the input domain (TBI images). We use a simulator [37] to generate a large collection of synthetic tumor images that resemble TBI images, and make use of the rich information in this database to automatically compute the likelihood density models, which are then transferred to the TBI domain.

We select a tumor image from the database that has the smallest earth mover's distance [38] compared to the input TBI images. We then obtain training samples in the known or "source" domain as a subset of the completely segmented tumor data $\{\hat{I}(\hat{x}),\hat{\ell}(\hat{x}),\hat{P}_c(\hat{x})\}$, with $\hat{I}$ representing the tumor intensities, $\hat{\ell}$ representing the discrete segmentations, $\hat{P}_c$ representing the probabilistic segmentations, and $\hat{x}$ representing the coordinates in the tumor image domain. The transfer of learned appearance models is accomplished via domain adaptation that incorporates importance weighting. We weight intensity observations I using the weights $w(I)=\frac{p(I)}{\hat{p}(I)}$ with $\hat{p}$ being the density in the source domain. In practice, w is estimated using KLIEP (Kullback–Leibler Importance Estimation Procedure) [39], which minimizes the Kullback–Leibler divergence between the density of the input domain and the weighted density of the source domain $KL(p(I)\parallel w(I)\,\hat{p}(I))$. Fig. 4 shows a toy example of applying KLIEP to estimate the weight. We observe the estimated weights are close to the true weights. Using the estimated weights w, we compute the density parameter $\hat{\theta}$ that maximizes the data likelihood in the tumor domain:

$$\underset{\hat{\theta}}{\operatorname{argmax}} \sum_{\hat{x}} w(\hat{I}(\hat{x}))\ \log\Big(\sum_c \hat{P}_c(\hat{x})\,\hat{p}(\hat{I}(\hat{x})|c,\hat{\theta}_c)\Big).$$

We use the kernel density model for the image appearance, parameterized by the kernel bandwidths for each class $\hat{\theta}=\{\hat{h}^{c=1},\ldots,\hat{h}^{c=C}\}$. The image likelihood in the TBI domain is modeled in the same fashion, where we initialize the TBI parameter θ using the "domain adapted" tumor parameter $\hat{\theta}$.

4. Results

4.1. Synthetic data analysis

Proof of concept of the new method is based on a synthetic longitudinal multimodal image data with two time points with pathologies. We simulate images with 4 channels (Ch1 to Ch4) and

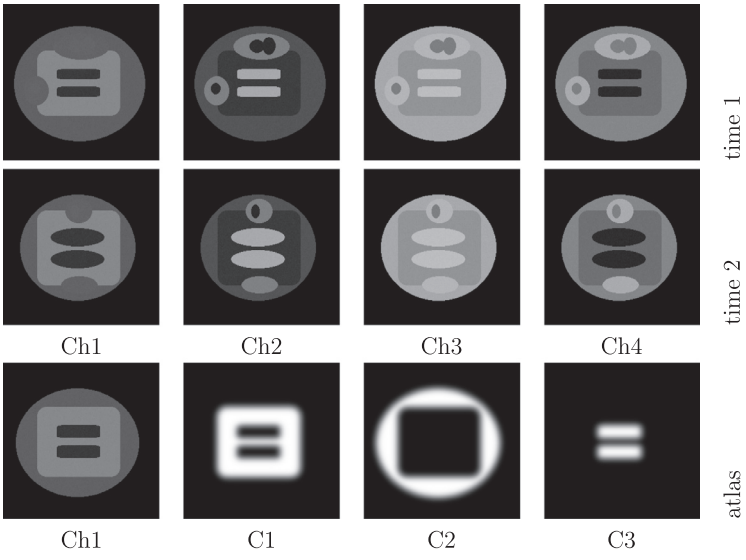

Fig. 5. Axial view of synthetic dataset for modal parameter analysis. Top to bottom: Multimodal images at time point 1, time point 2, and the co-registered atlas that represent only healthy classes but not pathology. Simulated pathology includes a deformable lesion (positioned at top within images), an appearing lesion (bottom location in images), and a disappearing lesion (left location in images). Please note that the atlas (bottom) does not provide spatial priors for lesions.

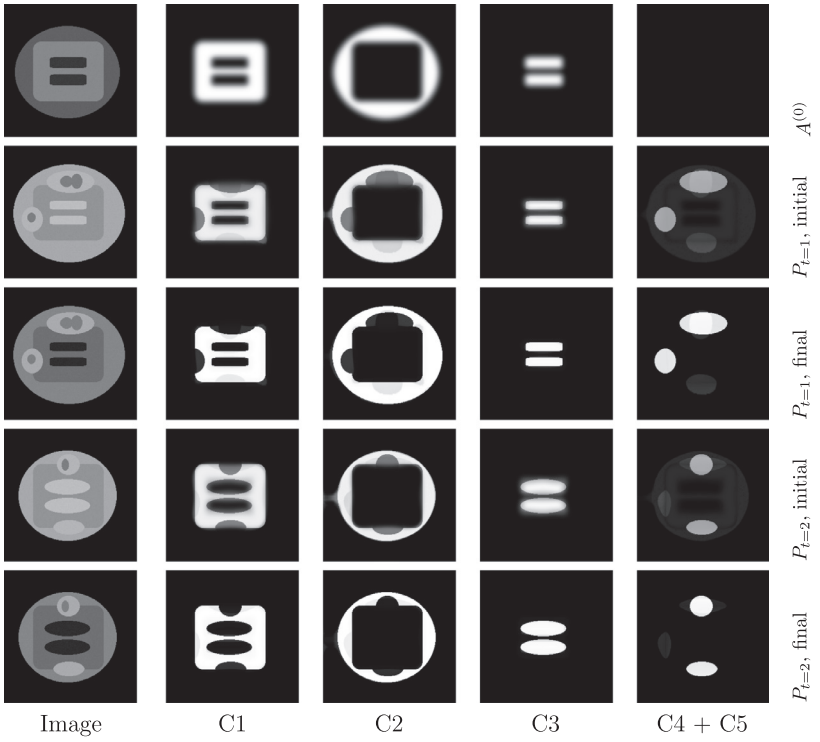

Fig. 6. Estimated 4D anatomical priors for synthetic data. First row shows the initial atlas $A^{(0)}$ in the template space, with the Ch1 channel image shown as a reference. Second and fourth rows show initial estimation (iteration 1 of the alternating gradient decent) of the personalized atlas $P_t = A \circ \phi_t + Q_t$ for time points 1 and 2, shown together with input channel Ch3. Third and fifth rows show the final estimation (iteration 16 of the alternating gradient decent) of the personalized atlas P_t for both time points, with the input Ch4 channel image shown as a reference.

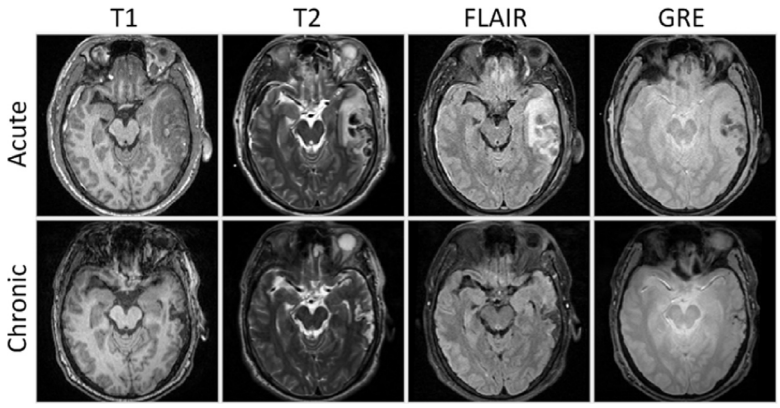

Fig. 7. Axial views of acute and chronic images of Subject I.

5 classes (C1 to C5) with class 4 and 5 mimicking behavior of two different new classes that are not represented in the atlas. In order to simulate the topological change problem, we create two types of changes of the fourth and fifth classes (C4 and C5). At the top of both time points, we simulate a deforming structure that changes shape. In the left of the images of time 1 and the bottom of the images of time 2, we simulate disappearing and newly appearing structures. Gaussian noise is added to the synthetic images for the purpose of simulation. In addition to this longitudinal synthetic dataset, we also create a normative atlas that contains the pair of multimodal images and priors for the first three classes (C1–C3) (Fig. 5).

We use the simulated dataset to illustrate the mechanism of the proposed algorithm, shown in Fig. 6. We observe that the initial estimates of posterior probabilities at each time point ($P_{t=1}$ and $P_{t=2}$) look like the mixture of the original atlas and data likelihood at the specific time point. The final estimation of the posteriors $P_{t=1}$ and $P_{t=2}$ becomes much more similar to the data likelihood at the specific time points, illustrating that the proposed method is able to account for topological changes across time although lesions are not modeled in the normative template.

4.2. Model parameter analysis

We apply our framework to multimodal image data of three TBI subjects. Each subject was scanned at two time points: an acute scan at ≈3 days and a chronic scan ≈ 6 months later. The image data of each subject include T1, T2, FLAIR, and GRE modalities. Acute and chronic images of Subject I are shown in Fig. 7 where nonhemorrhagic lesions (edema / swelling) are shown as hyperintense regions in FLAIR while hemorrhagic lesions (bleeding) are shown as hypointense regions in T2 and GRE.

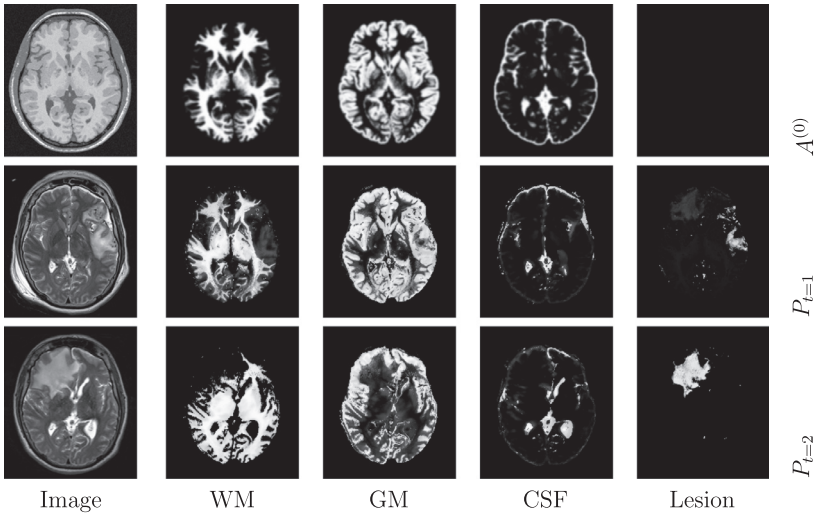

Fig. 8. Estimated 4D anatomical priors for TBI Subject II. First row shows the initial atlas $A^{(0)}$ in the template space, with the healthy T1 image as a reference. Second and third rows show the personalized atlas $P_t = A \circ \phi_t + Q_t$ for acute and chronic stages, with input T2 images shown. Our method is able to account for changes in the left-frontal and mid-frontal regions across time.

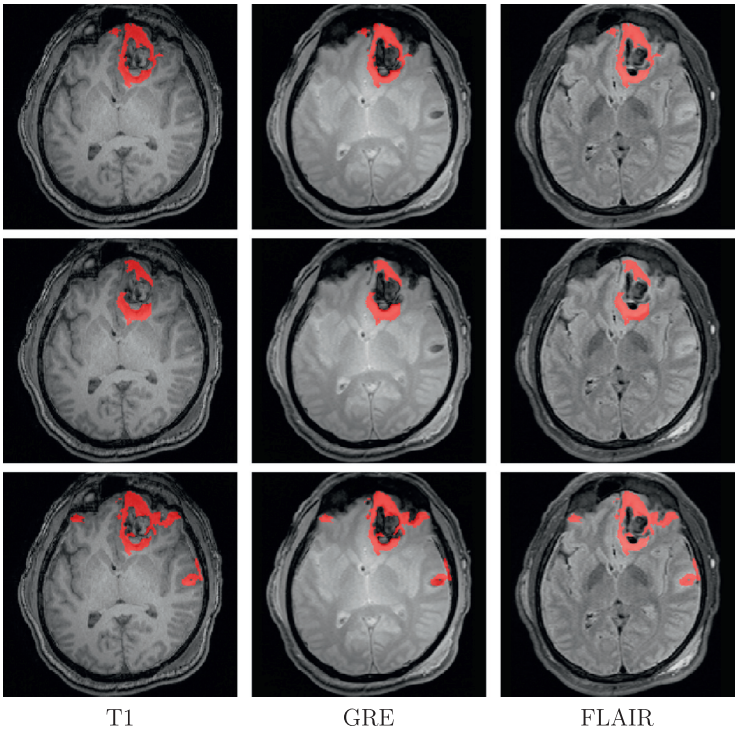

Fig. 9. Axial view of manual segmentation by three human experts for acute nonhemorrhagic lesions (NHL) of Subject III.

The estimated 4D spatial priors for TBI Subject II are illustrated in Fig. 8, incorporating template deformation to match image boundaries and nondiffeomorphic changes due to lesions. Subject II provides an interesting example of the complexity of longitudinal pathology progression. The acute scan reveals gross pathology in the left frontal region, which results in considerable atrophy in this region at the chronic stage. However, the subject's chronic scan features an additional large lesion in the mid-frontal region due to the occurrence of a large abscess between the acute and chronic scans. This is an excellent example of the dynamic and complex longitudinal changes that can occur in TBI patients.

4.3. Qualitative and quantitative evaluation of manual segmentation

Validation has been performed by a comparison of our results to expert segmentations. We asked three experts familiar with TBI lesion appearance to perform manual annotation using ITK-SNAP 3.2.0 [30], a new tool that provides simultaneous display of multimodality data along with user-guided 2D and 3D segmentation. We also explored the variability of human experts via qualitative and quantitative comparison.

Fig. 9 shows the axial view of edema manual segmentation of three human experts for the acute time point data of one subject. We clearly observe that the manual segmentations of three human

Table 1
Dice values comparing the acute NHL segmentation result of the six methods to the manual segmentations of the three human experts. Method I: no transfer learning and no atlas; Method II: transfer learning without atlas; Method III: transfer learning and atlas; Method IV: user initialization; Method V: GrabCut; Method VI: active learning-based user interaction (ActiveCut). Method I, II, V are baseline algorithms, the other three are the proposed methods for image appearance model learning.

Subject	Human Expert	Method					
		Noninteractive			Interactive		
		I	II	III	IV	V	VI
I	1	0.2006	0.2502	**0.3280**	**0.5177**	0.2503	**0.6349**
	2	0.1704	0.2477	**0.3312**	**0.5982**	0.2524	**0.7335**
	3	0.1880	0.2735	**0.3755**	**0.6087**	0.2712	**0.7928**
II	1	0.1456	0.1293	**0.1411**	**0.4835**	0.3269	**0.6910**
	2	0.1579	0.1309	**0.1464**	**0.4907**	0.3209	**0.7266**
	3	0.1896	0.1462	**0.1508**	**0.5451**	0.5241	**0.7720**
III	1	0.0224	0.0191	**0.0231**	**0.3226**	0.1311	**0.4511**
	2	0.0004	0.0002	**0.0002**	**0.1935**	0.0915	**0.4611**
	3	0.0111	0.0025	**0.0026**	**0.4094**	0.1083	**0.4608**

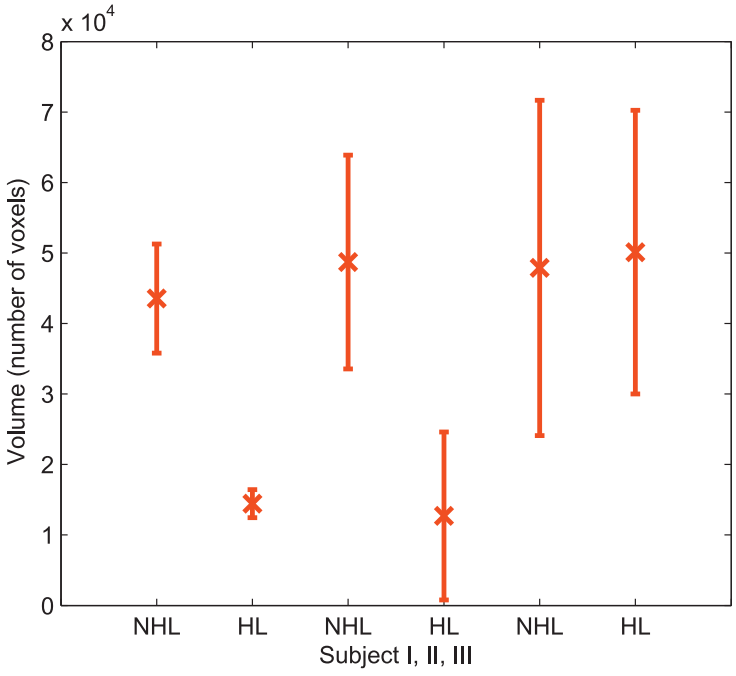

Fig. 10. Mean and standard deviation of manual annotations from three human experts for acute hemorrhagic lesion (HL) and nonhemorrhagic lesion (NHL) of subjects I, II, and III.

experts show some variability regarding lesion boundaries but also the number of lesions. The manual segmentations of the first two rows cover the major site of edema; however, the result in the third row includes two additional lesions apart from the major site (top-left and middle-right in the third row images). Moreover, even if the results of the first two rows look similar, the volumes are significantly different. Fig. 10 shows the acute lesion volume averages of three subjects with standard deviation bars. We observe a relatively large standard deviation that reflects the significant variability and disagreement of manual segmentation by different human experts. These qualitative and quantitative results provide evidence that TBI lesion segmentation is a difficult task for experts even using new tools that offer multimodality displays.

4.4. Qualitative and quantitative evaluation of automatic segmentation

As introduced in the method section, we provide three possibilities for initialization of image appearance models: user initialization via regions of interest, iterative user interaction (ActiveCut), and fully automatic transfer learning. In order to illustrate the performance of the proposed method, we compare our method to (1) appearance model estimation without transfer learning, which uses the same training dataset as our method of learning with transfer learning; (2) appearance model learning with transfer learning but without an atlas; (3) the GrabCut segmentation without iterative updates but allowing the foreground to be segmented as background classes. The three methods are used as the baseline algorithms to compare with our three image appearance model learning methods.

Since we have three independent manual segmentations for each subject, each human expert's manual segmentations are used to compare with the segmentation results of different methods. We validate the performance of different methods by comparing the segmentation to the selected manual segmentation. We use the Dice coefficient as our comparison metric, which measures the volumetric overlap of two binary segmentations and lies in [0, 1].

Table 1 shows the comparisons of the results of our methods and three baseline algorithms against the three independent manual segmentations. The Dice coefficient values are relatively low

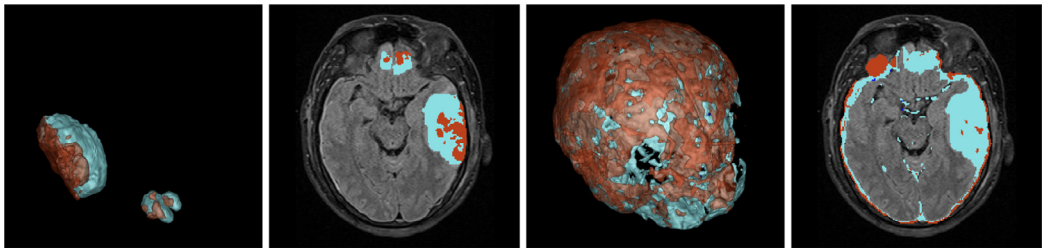

Fig. 11. Comparison between GrabCut and our active learning-based method. Left: our method in 3D space and axial view. Right: GrabCut. Light blue: edema. Brown: bleeding. Note the large false-positive detection of GrabCut in the CSF region. (For interpretation of the references to color in this figure legend, the reader is referred to the web version of this article.)

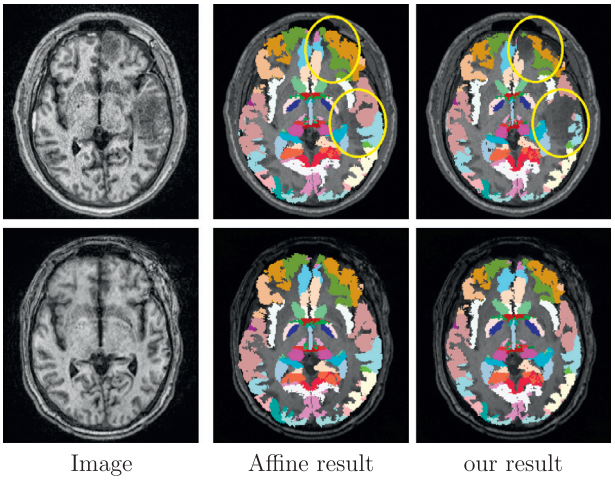

Fig. 12. Example of brain parcellation labels mapped to the acute (first row) and chronic (second row) time points of Subject I.

due to the complex shapes of the small lesions, but the importance is the difference between the baseline methods and ours. In general, we observe that the performance of our method varies with different image appearance model estimations. The Dice values increase from fully automatic transfer learning-based initialization to semiautomatic user initialization, to active learning-based user interaction. The growth of Dice values is reasonable as the algorithm gets increasingly better training data. We may not conclude that the transfer learning-based initialization would be poor since it provides a fully automatic solution with the cost that the segmentation accuracy may be less optimal. On the other hand, even if the result of the active learning-based method is the best in terms of segmentation accuracy, it requires users to do iterative interaction for each dataset. Such a procedure may be appropriate for a small sample set but may not be suitable for large population studies.

Fig. 11 shows the qualitative comparison between GrabCut and our active learning-based method (ActiveCut). Without user interaction, the baseline algorithm detected a large number of false-positive voxels due to the ambiguity between lesion and non-brain tissue or fluid.

4.5. Result of brain parcellation

The proposed method has the advantage of providing a mapping from a normative template to a specific subject. In Fig. 12, we show the brain parcellation label image, provided by the International Consortium for Brain Mapping (ICBM), mapped to the acute (first row) and chronic (second row) time points of one TBI subject using affine registration and our method. We observe that our method produces more accurate mapping from healthy brain atlas to individual time points of a TBI subject.

In Fig. 13, we illustrate another result of mapping the ICBM parcellation label image to a TBI subject with both 2D and 3D visualizations. The mapping of a normal anatomy to a pathological anatomy will be potentially important to compare type, locality, and spatial extent of brain damage in the context of anatomically relevant regions with associated brain function information.

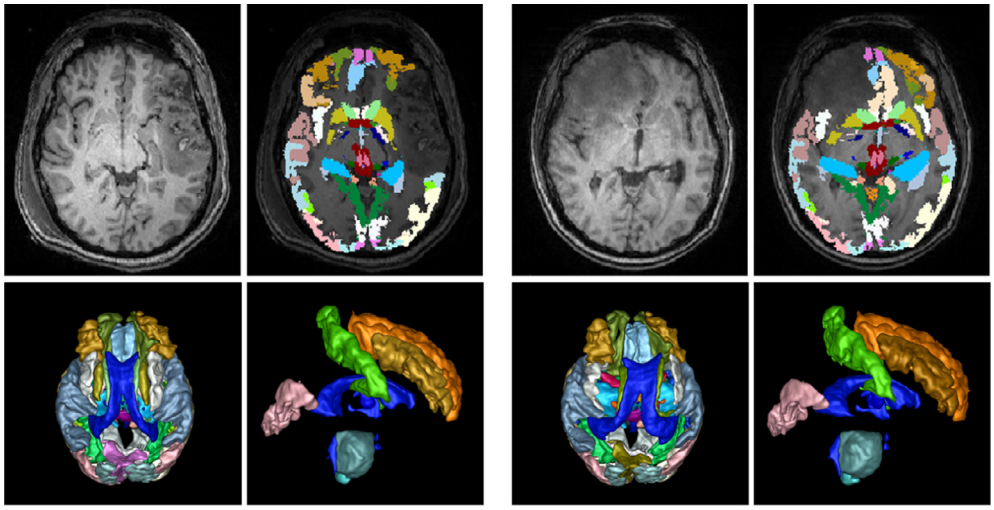

Fig. 13. Example of brain parcellation labels mapped to the acute (left) and chronic (right) time points of Subject II. For each time point, we show the input T1 image and the overlaid parcellation labels. Our method generates parcellation maps that match tissue boundaries and account for lesions.

5. Conclusions

We have presented a new framework that models 4D changes in pathological anatomy over time and provides explicit deformable mapping from a healthy template to subjects with pathology. The novel idea for registration of images with lesions is the estimation of spatial class priors as a combination of diffeomorphic atlas deformation and nondiffeomorphic changes of lesion probabilities. This concept enables intrasubject registration of longitudinal images with spatially and temporally varying lesion patterns but also a mapping of a normative atlas to subject images. To overcome the shortcomings of atlas-based segmentation, which cannot be applied to images with new structures that are not represented in the template, our framework uses semisupervised learning approaches to get training data for Gaussian mixture models by user initialization or active learning-based user interaction. We also discuss the use of a transfer learning method that results in a fully automatic 4D segmentation method. The feasibility of our approach is demonstrated with synthetic data and 4D multimodal MR data of patients with severe TBI.

The novel joint segmentation-registration method for longitudinal image data provides not only change trajectories of lesions but also simultaneous segmentation of normal-appearing tissue classes. We thus provide 4D spatiotemporal models of pathological anatomy and information on tissue fate profiles and lesion changes, which will be relevant for clinical assessment of therapeutic intervention but are not yet available in clinical practice.

We include a preliminary validation by comparing automatic or automated segmentation to the results of three expert raters. Even with experts familiar with reading multimodal MR images of TBI subjects and applying the updated ITK-SNAP tool designed for user-guided multimodal image analysis, we observe relatively large inter-rater variability. Such disagreement between raters will represent a fundamental limitation of the proposed quantitative analysis as there is no clear notion of a ground truth for lesions. We have performed validation limited to three subjects where multimodal longitudinal data was available. As part of our multicenter collaboration, we plan to extend validation and testing to a larger cohort.

Our proposed method has potential applications for brain mapping, but now in the presence of large pathologies, as it registers a normative template to each individual time point, the template-based parcellation of each subject facilitates analysis of structural brain connectivity with diffusion imaging. Progress on connectivity analysis has so far been held up by the fact that well-established processing pipelines do not work on image data presenting mass-occupying lesions and infiltrations. Researchers therefore had to go through tedious and time-consuming manual editing, requiring hours to days per dataset, in order to pre-process image data. In the future, we plan to demonstrate the use of our framework for conducting regional analysis similar to the one performed by [2], where TBI subjects are labeled appropriately without manual editing. The spatiotemporal model obtained through our framework also provides measures of change in normal-appearing tissue, e.g., loss of gray matter and reduction of cortical thickness. Such measures will provide quantitative parameters for monitoring the trajectory of TBI rehabilitation in addition to lesion delineation, as shown in our previous work [40] on identifying biomarkers for patient recovery.

Acknowledgments

Supported by grants: National Alliance for Medical Image Computing (NA-MIC) U54 EB005149 (GG) and the Utah Science Technology and Research (USTAR) initiative at the University of Utah.

Appendix A. Derivation of update equations

We can rewrite $\mathcal{F}(A, \phi_t, Q_t)$ as

$$\mathcal{F} = -\sum_{t=1}^{T}\sum_{x=1}^{N} \log\left(\sum_{c=1}^{C}\left(A^c(x)\circ\phi_t(x) + Q_t^c(x)\right) p(I_t(x)|c,\theta_t^c)\right), \tag{A.1}$$

which is defined in subject space I_t. Alternatively, we can define this functional in the atlas space A,

$$\mathcal{F}\circ\phi_t^{-1} = -\sum_{t=1}^{T}\sum_{x=1}^{N} \log\Bigg(\sum_{c=1}^{C}(A^c(x) + Q_t^c(x)\circ\phi_t^{-1}(x)) \times p(I_t(x)\circ\phi_t^{-1}(x)|c,\theta_t^c)\Bigg). \tag{A.2}$$

The updated for Q is obtained through the derivative of the functional in subject space I_t,

$$\nabla_{Q_t^c}\mathcal{F}(x) = -\frac{p(I_t(x)|c,\theta_t^c)}{\sum_{c'}(A^{c'}(x)\circ\phi_t(x) + Q_t^{c'}(x))\, p(I_t(x)|c',\theta_t^{c'})}. \tag{A.3}$$

The update for A is obtained through a change of coordinates,

$$\begin{aligned}\nabla_{A^c}\mathcal{F}(x) &= \left[\nabla_{A^c}\mathcal{F}\circ\phi_t^{-1}\right]|D\,\phi_t(x)|,\\ &= -\sum_{t}\frac{|D\,\phi_t(x)|\, p(I_t(\phi_t^{-1}(x))|c,\theta_t^c)}{\sum_{c'}(A^{c'}(x) + Q_t^{c'}(\phi_t^{-1}(x)))\, p(I_t(\phi_t^{-1}(x))|c',\theta_t^{c'})}.\end{aligned} \tag{A.4}$$

The update for ϕ is obtained through the functional derivative of ϕ in subject space I_t,

$$\nabla_{\phi_t}\mathcal{F}(x) = -\sum_{c}\frac{p(I_t(x)|c,\theta_t^c)}{\sum_{c'}(A^{c'}(x)\circ\phi_t(x) + Q_t^{c'}(x))\, p(I_t(x)|c',\theta_t^{c'})} \times \nabla(A^c\circ\phi_t(x)), \tag{A.5}$$

References

[1] A. Irimia, M.C. Chambers, J.R. Alger, M. Filippou, M. Prastawa, B. Wang, D.A. Hovda, G. Gerig, A.W. Toga, R. Kikinis, P.M. Vespa, J.D.V. Horn, Comparison of acute and chronic traumatic brain injury using semi-automatic multimodal segmentation of MR volumes, J.Neurotrauma 28 (2011) 2287–2306.
[2] A. Irimia, B. Wang, S. Aylward, M. Prastawa, D. Pace, G. Gerig, D. Hovda, R. Kikinis, P. Vespa, J. Van Horn, Neuroimaging of structural pathology and connectomics in traumatic brain injury: Toward personalized outcome prediction, NeuroImage: Clin. 1 (1) (2012) 1–17.
[3] M. Faul, L. Xu, M. Wald, V. Coronado, Traumatic Brain Injury in the United States: Emergency Department Visits, Hospitalizations and Deaths 2002-2006. National Center for Injury Prevention and ControlAtlanta (GA): CDC, 2010.
[4] M. Datar, J. Cates, P.T. Fletcher, S. Gouttard, G. Gerig, R. Whitaker, Particle based shape regression of open surfaces with applications to developmental neuroimaging, in: Proceedings of the Medical Image Computing and Computer-Assisted Intervention–MICCAI 2009, Springer, 2009, pp. 167–174.
[5] P.T. Fletcher, Geodesic regression and thetheory of least squares on riemannian manifolds, Int. J. Comput. Vis. 105 (2) (2012) 1–15.
[6] M. Niethammer, Y. Huang, F.-X. Vialard, Geodesic regression for image time-series, in: Proceedings of the Medical Image Computing and Computer-Assisted Intervention–MICCAI 2011, Springer, 2011, pp. 655–662.
[7] J. Fishbaugh, M. Prastawa, G. Gerig, S. Durrleman, Geodesic shape regression in the framework of currents, in: Proceedings of the Information Processing in Medical Imaging, Springer, 2013, pp. 718–729.
[8] Y. Hong, S. Joshi, M. Sanchez, M. Styner, M. Niethammer, Metamorphic geodesic regression, in: Proceedings of the Medical Image Computing and Computer-Assisted Intervention–MICCAI 2012, Springer, 2012, pp. 197–205.
[9] B.H. Menze, K. Van Leemput, D. Lashkari, M.-A. Weber, N. Ayache, P. Golland, A generative model for brain tumor segmentation in multi-modal images, in: Proceedings of the Medical Image Computing and Computer-Assisted Intervention–MICCAI 2010, Springer, 2010, pp. 151–159.
[10] E. Geremia, O. Clatz, B.H. Menze, E. Konukoglu, A. Criminisi, N. Ayache, Spatial decision forests for ms lesion segmentation in multi-channel magnetic resonance images, NeuroImage 57 (2) (2011) 378–390.
[11] S. Bauer, L.-P. Nolte, M. Reyes, Fully automatic segmentation of brain tumor images using support vector machine classification in combination with hierarchical conditional random field regularization, in: Proceedings of the Medical Image Computing and Computer-Assisted Intervention–MICCAI 2011, 2011, pp. 354–361.

[12] Y. Gao, R. Kikinis, S. Bouix, M. Shenton, A. Tannenbaum, A 3D interactive multi-object segmentation tool using local robust statistics driven active contours, Med. Image Anal. 16 (6) (2012) 1216–1227.
[13] C. Ledig, R.A. Heckemann, A. Hammers, J.C. Lopez, V.F. Newcombe, A. Makropoulos, J. Lötjönen, D.K. Menon, D. Rueckert, Robust whole-brain segmentation: Application to traumatic brain injury, Med. Image Anal. 21 (1) (2015) 40–58.
[14] K.V. Leemput, F. Maes, D. Vandermeulen, P. Suetens, Automated model-based tissue classification of MR images of the brain, IEEE Trans. Med. Imaging 18 (10) (1999) 897–908.
[15] M. Prastawa, E. Bullitt, N. Moon, K. Van Leemput, G. Gerig, Automatic brain tumor segmentation by subject specific modification of atlas priors, Acad. Radiol. 10 (12) (2003) 1341–1348.
[16] N. Chitphakdithai, J.S. Duncan, Non-rigid registration with missing correspondences in preoperative and postresection brain images, in: Proceedings of the MICCAI, 2010, pp. 367–374.
[17] M. Niethammer, G.L. Hart, D.F. Pace, P.M. Vespa, A. Irimia, J.D.V. Horn, S.R. Aylward, Geometric metamorphosis, in: Proceedings of the MICCAI (2), 2011, pp. 639–646.
[18] Y. Ou, A. Sotiras, N. Paragios, C. Davatzikos, DRAMMS: Deformable registration via attribute matching and mutual-saliency weighting, Med. Image Anal. 15 (4) (2011) 622–639.
[19] Y. Lou, A. Irimia, P. Vela, M. Chambers, J. Van Horn, P. Vespa, A. Tannenbaum, Multimodal deformable registration of traumatic brain injury MR volumes via the Bhattacharyya distance, IEEE Trans. Med. Imag. 60 (9) (2013) 2511–2520.
[20] S.K. Kyriacou, C. Davatzikos, S.J. Zinreich, R.N. Bryan, Nonlinear elastic registration of brain images with tumor pathology using a biomechanical model, IEEE Trans. Med. Imag., 18 (7) (1999) 580–592.
[21] M.B. Cuadra, C. Pollo, A. Bardera, O. Cuisenaire, J.-G. Villemure, J. Thiran, Atlas-based segmentation of pathological MR brain images using a model of lesion growth, IEEE Trans. Med. Imag., 23 (10) (2004) 1301–1314.
[22] E.I. Zacharaki, D. Shen, S.-K. Lee, C. Davatzikos, ORBIT: a multiresolution framework for deformable registration of brain tumor images, IEEE Trans. Med. Imag., 27 (8) (2008) 1003–1017.
[23] B.H. Menze, K.V. Leemput, A. Honkela, E. Konukoglu, M. Weber, N. Ayache, P. Golland, A generative approach for image-based modeling of tumor growth, in: Proceedings of the 22nd International Conference, IPMI Information Processing in Medical Imaging, 2011, pp. 735–747.
[24] A. Gooya, K.M. Pohl, M. Bilello, L. Cirillo, G. Biros, E.R. Melhem, C. Davatzikos, Glistr: Glioma image segmentation and registration., IEEE Trans. Med. Imaging 31 (10) (2012) 1941–1954.
[25] K.M. Pohl, J. Fisher, W.E.L. Grimson, R. Kikinis, W.M. Wells, A bayesian model for joint segmentation and registration, NeuroImage 31 (1) (2006) 228–239.
[26] S. Parisot, W.W. III, S. Chemouny, H. Duffau, N. Paragios, Concurrent tumor segmentation and registration with uncertainty-based sparse non-uniform graphs, Med. Image Anal. 18 (4) (2014) 647–659.
[27] D. Kwon, M. Niethammer, H. Akbari, M. Bilello, C. Davatzikos, K. Pohl, Portr: Pre-operative and post-recurrence brain tumor registration, IEEE Trans. Med. Imaging 33 (3) (2014) 651–667.
[28] X. Liu, M. Niethammer, R. Kwitt, M. McCormick, S. Aylward, Low-rank to the rescue – atlas-based analyses in the presence of pathologies, in: Proceedings of the International Conference on Medical Image Computing and Computer Assisted Intervention (MICCAI), 2014.
[29] B. Wang, M. Prastawa, A. Saha, S.P. Awate, A. Irimia, M.C. Chambers, P.M. Vespa, J.D. Van Horn, V. Pascucci, G. Gerig, Modeling 4D changes in pathological anatomy using domain adaptation: Analysis of tbi imaging using a tumor database, in: Proceedings of the Multimodal Brain Image Analysis, Springer, 2013, pp. 31–39.
[30] P.A. Yushkevich, J. Piven, H.C. Hazlett, R.G. Smith, S. Ho, J.C. Gee, G. Gerig, User-guided 3d active contour segmentation of anatomical structures: significantly improved efficiency and reliability, Neuroimage 31 (3) (2006) 1116–1128.
[31] M. Prastawa, S. Awate, G. Gerig, Building spatiotemporal anatomical models through joint segmentation, registration, and 4D-atlas estimation, in: Proceedings of the MMBIA, 2012, pp. 49–56.
[32] M. Prastawa, E. Bullitt, S. Ho, G. Gerig, A brain tumor segmentation framework based on outlier detection., Med. Image Anal. 8 (3) (2004) 275–283.
[33] B. Wang, M. Prastawa, S.P. Awate, A. Irimia, M.C. Chambers, P.M. Vespa, J.D. Van Horn, G. Gerig, Segmentation of serial MRI of TBI patients using personalized atlas construction and topological change estimation, in: Proceedings of the 9th International Symposium on Biomedical Imaging (ISBI), 2012, IEEE, 2012, pp. 1152–1155.
[34] S.P. Lloyd, Least squares quantization in pcm, IEEE Trans. Inf. Theory 28 (1982) 129–137.
[35] B. Wang, W. Liu, M. Prastawa, A. Irimia, P.M. Vespa, J.D. van Horn, P.T. Fletcher, G. Gerig, 4D active cut: An interactive tool for pathological anatomy modeling, in: Proceedings of the IEEE 11th International Symposium on Biomedical Imaging (ISBI), 2014, IEEE, 2014, pp. 529–532.
[36] C. Rother, V. Kolmogorov, A. Blake, Grabcut: Interactive foreground extraction using iterated graph cuts, ACM TOG 23 (2004) 309–314.
[37] M. Prastawa, E. Bullitt, G. Gerig, Simulation of brain tumors in MR images for evaluation of segmentation efficacy, Med. Image Anal. 13 (2) (2009) 297–311.
[38] O. Pele, M. Werman, Fast and robust earth mover's distances, in: Proceedings of the 12th International Conference on Computer vision, 2009, IEEE, 2009, pp. 460–467.
[39] M. Sugiyama, S. Nakajima, H. Kashima, P. Von Buenau, M. Kawanabe, Direct importance estimation with model selection and its application to covariate shift adaptation, Adv. NIPS 20 (2008) 1433–1440.
[40] B. Wang, M. Prastawa, A. Irimia, M.C. Chambers, N. Sadeghi, P.M. Vespa, J.D. Van Horn, G. Gerig, Analyzing imaging biomarkers for traumatic brain injury using 4d modeling of longitudinal MRI, in: Proceedings of the 2013 IEEE 10th International Symposium on Biomedical Imaging (ISBI), IEEE, 2013, pp. 1392–1395.